PHYSICAL REVIEW A **86**, 053413 (2012)

# Test of the Stark-effect theory using photoionization microscopy

L. B. Zhao,[1] I. I. Fabrikant,[1] M. L. Du,[2] and C. Bordas[3]
[1] *Department of Physics and Astronomy, University of Nebraska, Lincoln, Nebraska 68588-0299, USA*
[2] *Institute of Theoretical Physics, Chinese Academy of Sciences, P. O. Box 2735, Beijing 100190, China*
[3] *Université Lyon I, LASIM, UMR CNRS 5579, 43 Boulevard du 11 Novembre 1918, F69622 Villeurbanne Cedex, France*

(Received 9 August 2012; published 26 November 2012)

We formulate the dynamics of electron-wave propagation in photoionization microscopy for nonhydrogenic atoms, based on a frame transformation between the spherical and parabolic coordinates used in Harmin's Stark-effect theory. An expression for the wave function for photoelectrons ejected from the nonhydrogenic atomic source has been derived. The spatial distributions of electron current densities or differential cross sections for Na are computed and compared to those from a recently developed coupled-channel theory. The difference between these two approaches is analyzed and attributed to the frame transformation for irregular wave functions. Since more detailed physical information can be extracted by comparing differential cross sections, rather than total cross sections, photoionization microscopy is proposed to test the Stark-effect theory.

DOI: 10.1103/PhysRevA.86.053413 PACS number(s): 32.80.Fb, 07.81.+a

## I. INTRODUCTION

Investigation of dynamical properties of Rydberg atoms and molecules in an external electric field has attracted much attention for decades due to fundamental physics interest in such systems themselves and their potential applications in other research fields. So far, a great deal of experimental and theoretical effort has been spent to understand the behavior of Rydberg atoms and molecules in external electric fields (see, e.g., Refs. [1,2] and references therein). Pronounced asymmetrical line shapes were found in experimental photoionization spectra for several nonhydrogenic atoms [3–5], and explained by Harmin's Stark-effect theory in the WKB approximation [6–8]. These profiles were thought to be due to interference between continuum and quasidiscrete states similarly to field-free Fano profiles. Furthermore, it was found that these experimental spectra exhibit series of polarization-dependent oscillations, and these oscillations in the Rydberg-energy region extend beyond the field-free threshold. This phenomenon was explained by Harmin's theory. Each peak in the spectra is related to a resonance specified by the parabolic quantum number $n_1$ and magnetic quantum number $m$, and the oscillations above the field-free threshold are induced by the external electric field. In addition, the closed-orbit theory developed by Du and Delos [9] also successfully interprets such oscillations [10].

As displayed in the experimental photoionization spectra, a Stark resonance may be broad or narrow, depending on the energy and the electric field. The long-lifetime feature of a narrow resonance may be exploited for many research purposes, such as precise calibrations of applied electric fields [11–13], and trapping of Rydberg atoms and molecules [14], which may be used for Bose-Einstein condensates [15], studies of cold molecular collisions [16], and quantum information processing [17]. Another peculiar feature of the Stark effect arises from the tunability of the electric field and of the corresponding couplings. In some circumstances this can lead to the stabilization of states in the continuum. As an example, an extremely narrow Stark resonance in sodium atoms was experimentally observed and interpreted by Harmin's theory [11]. This resonance is located near $-184$ cm$^{-1}$, where two relatively broad resonances cross, and one of them is narrowed by two to three orders of magnitude due to interference between quasidiscrete and continuum states, in the presence of electric fields with strength 3950 V/cm. A subsequent investigation of sodium Stark resonances shows that interference narrowing may increase a resonance lifetime by up to four orders of magnitude over a normal lifetime of 0.02–0.10 ns [12]. Thus the lifetime of a stabilized Stark resonance may be as long as 100 ns.

Recently, a precise spectroscopic measurement with an accompanying theoretical analysis of the Stark effect for neon in a static electric field has been presented [2]. The theoretical analysis was based on the multichannel quantum-defect theory (MQDT) to treat the Stark effect in Rydberg states [18,19], and the MQDT was developed from Harmin's Stark-effect theory using a frame transformation between spherical and parabolic coordinates. Discrepancies between experiment and theory near the Stark resonances were observed, and were suspected to be due to the neglect of the field effect beyond the core region with $r \ll \mathscr{F}^{-1/2}$ ($\mathscr{F}$ is the electric-field strength). Such discrepancies indicate the necessity of reexamination of the approximations made in the MQDT approach, and the authors of Ref. [2] suggested that it might be necessary to develop new methodologies to incorporate the field effect near the core into the MQDT framework.

Harmin's Stark-effect theory was also questioned by Stevens *et al.* [13]. It was found that the frame transformation of irregular wave functions defined in this theory does not maintain consistency in the two sides of the transformation equation. One side of the transformation equation is phase shifted isotropically, while the other side is phase shifted on the negative $z$ axis but not on the positive $z$ axis. However, as indicated above, Harmin's Stark-effect theory turns out to be successful in reproducing the experimental photoionization spectrum for Na in an electric field. Obviously, it is essential to develop a theoretical scheme, which should provide more detailed comparison, to examine Harmin's Stark-effect theory. Photoionization microscopy [20,21] is able to satisfy this requirement. By comparing electron current densities or detailed differential cross sections, instead of total cross sections, one can scrutinize Harmin's Stark-effect theory. Such a test is the aim of the present paper. For this purpose, it is necessary to formulate the dynamics of electron-wave propagation in photoionization microscopy for nonhydrogenic atoms, based on the frame transformation between the spherical and parabolic coordinates used in Harmin's Stark-effect theory.

A theoretical approach to simulate time-dependent electron currents produced in photoionization of nonhydrogenic atoms in a static electric field has been formulated by Robicheaux and Shaw [22], based on Harmin's theory in the WKB approximation [8]. They semiclassically computed electron wave functions in the Coulomb-Stark potential and the frame-transformation matrix which connects wave functions in spherical and parabolic coordinates. In the present paper, however, these quantities will be calculated by numerical solution of the Schrödinger equation rather than by the WKB approximation. Specifically, the effects of Stark resonances are calculated within the framework of fully quantum-mechanical theory. We find that the treatment of the frame transformation of irregular wave functions in Harmin's Stark-effect theory may need to be improved.

The paper is organized as follows. In Sec. II, Harmin's Stark-effect theory is reviewed. In Sec. III, we derive the expression for outgoing electron waves produced in photoionization for nonhydrogenic atoms in a uniform electric field, based on Harmin's Stark-effect theory. In Sec. IV, computations of the transformation matrices between parabolic regular and irregular wave functions proposed by Harmin [8] in the WKB framework are outlined, and some computed examples from the fully quantum-mechanical theory are listed. Section V presents spatial distributions of current densities produced due to photoionization of Na atoms from the ground state through the intermediate $3\,^2P_{3/2}$ state in electric fields. Section VI summarizes the approach of photoionization microscopy for nonhydrogenic atoms developed to test Harmin's Stark-effect theory, and the main conclusion. Atomic units are used throughout this paper unless otherwise noted.

## II. REVIEW OF HARMIN'S STARK-EFFECT THEORY

### A. Sketch of the theory

This section sketches Harmin's Stark-effect theory, and summarizes formulas relevant to the current derivation of the outgoing electron wave function. We use the same symbols as Harmin wherever possible. Let the configuration space be divided into three parts: the core region with $r < r_0$, the Coulomb region with $r_0 < r < r_1$, and the Coulomb-Stark region with $r > r_1$. The value of $r_1$ is taken from the range $r_0 \ll r \ll \mathscr{F}^{-1/2}$, where $\mathscr{F}$ represents the electric-field strength, while $r_0$ is a few bohrs from the origin. The complicated dynamics happens in the core region, while the ejected electron experiences only the Coulomb force in the Coulomb region, since the uniform electric field is negligible at $r < r_1$. In the Coulomb-Stark region, the electron moves in the Coulomb and uniform electric fields. We start first with hydrogenic atoms and then switch to nonhydrogenic atoms with cores.

The Schrödinger equation for the H atom in a uniform external electric field is separable in parabolic coordinates, $\xi = r + z$, $\eta = r - z$, and $\phi = \tan^{-1}(y/x)$. Let us denote the energy-normalized solutions to the Schrödinger equation, regular at $r = 0$, as

$$\psi_{\epsilon n_1 m}(\xi,\eta,\phi) = \frac{u_\beta(\xi)}{\sqrt{\xi}}\frac{v_\beta(\eta)}{\sqrt{\eta}}\frac{e^{im\phi}}{\sqrt{2\pi}}, \tag{1}$$

where $\epsilon$ is the energy of the electron, $n_1$ is the node number of $u(\xi)$, $m$ is the magnetic quantum number, and $\beta$ is the separation constant. $u_\beta(\xi)$ and $v_\beta(\eta)$ satisfy the ordinary differential equations

$$\left(\frac{d^2}{d\xi^2} + \frac{1-m^2}{4\xi^2} + \frac{\beta}{\xi} + \frac{\epsilon}{2} - \frac{\mathscr{F}}{4}\xi\right) u_\beta(\xi) = 0, \tag{2}$$

$$\left(\frac{d^2}{d\eta^2} + \frac{1-m^2}{4\eta^2} + \frac{1-\beta}{\eta} + \frac{\epsilon}{2} + \frac{\mathscr{F}}{4}\eta\right) v_\beta(\eta) = 0. \tag{3}$$

From the above two equations, one readily sees that $\beta$ is an implicit function of four parameters $\epsilon$, $\mathscr{F}$, $n_1$, and $m$, namely, $\beta(\epsilon,\mathscr{F},n_1,m)$. Therefore, $\beta$ represents the four indices, and to simplify the notation, we write $\beta$ without arguments. The forms of Eqs. (2) and (3) together with the boundary conditions show that $u_\beta(\xi) \to 0$ as $\xi \to \xi_0$, where $\xi_0$ is a finite value, while $v_\eta(\eta)$ is oscillatory as $\eta \to \infty$. Near the origin, the behavior of regular solutions of Eqs. (2) and (3) with energy-independent normalization is as follows:

$$u(\xi \sim 0) = N_\xi \xi^{(1+m)/2}[1 + O(\xi)], \tag{4}$$

$$v(\eta \sim 0) = N_\eta \eta^{(1+m)/2}[1 + O(\eta)], \tag{5}$$

where $N_\xi$ and $N_\eta$ are normalization amplitudes. $u(\xi)$ satisfies the normalization condition

$$\int_0^\infty \frac{u_{n_1}(\xi)u_{n_1'}(\xi)}{\xi} d\xi = \delta_{n_1 n_1'}, \tag{6}$$

and $v(\eta)$ has asymptotic behavior at $\eta \to \infty$,

$$v(\eta) \to \sqrt{\frac{2}{\pi k(\eta)}} \sin\left(\int^\eta k(\eta')d\eta' + \frac{1}{4}\pi + \delta_\beta\right), \tag{7}$$

where $k(\eta)$ represents the WKB wave number, and $\delta_\beta$ is the absolute phase shift. The lower limit of the integration in the phase integral of Eq. (7) is arbitrary, but the phase shift $\delta_\beta$ depends on its specific choice. Equations (4)–(7) are essential to calculate frame-transformation matrices. As in the treatment in parabolic coordinates, the normalization amplitude $N_{\epsilon\ell}$ in spherical coordinates can be factored out from the zero-field spherical functions, $\mathcal{F}_{\epsilon\ell m}(\mathbf{r})$ (see Ref. [8] for details). The transformation matrix $U_{\beta\ell}$ is defined by the equation

$$\psi_{\epsilon n_1 m}(\mathbf{r}) = \sum_\ell U_{\beta\ell}\mathcal{F}_{\epsilon\ell m}(\mathbf{r}), \tag{8}$$

and is given by

$$U_{\beta\ell} = a_{\beta\ell}\frac{N_\xi N_\eta}{N_{\epsilon\ell}}, \tag{9}$$

where $a_{\beta\ell}$ is the transformation coefficient. From its expression [Eq. (17) of Ref. [8]], it is easy to see that this coefficient itself is free from effects of the Stark and Coulomb potentials, and their effects on the transformation matrix are embodied in the normalization amplitudes $N_\xi$, $N_\eta$, and $N_{\epsilon\ell}$. It must be emphasized that the transformation of the wave functions between parabolic and spherical coordinates is valid only for the Coulomb region for any $\beta$ and $\ell$. In the Coulomb-Stark region, where the electric field is no longer negligible, the Hamiltonian is not separable in spherical coordinates, and as a consequence, the parabolic eigenfunction cannot be obtained in terms of the frame transformation. That means that $U_{\beta\ell}$ is nonorthogonal at fixed $\epsilon$, except for the field-free case.

If the region with $r \leqslant r_0$ is occupied by an alkali-metal ion core instead of a bare nucleus, the wave functions in the Coulomb region, outside the core boundary $r_0$, is written in the form

$$\overline{\Theta}_{\epsilon\ell m}(\mathbf{r}) = \cos\delta_\ell \mathcal{F}_{\epsilon\ell m}(\mathbf{r}) - \sin\delta_\ell \mathcal{G}_{\epsilon\ell m}(\mathbf{r}), \tag{10}$$

with the notation

$$\mathcal{F}_{\epsilon\ell m}(\mathbf{r}) = \frac{1}{r} f_{\epsilon\ell}(r) Y_{\ell m}(\theta,\phi), \tag{11}$$

$$\mathcal{G}_{\epsilon\ell m}(\mathbf{r}) = \frac{1}{r} g_{\epsilon\ell}(r) Y_{\ell m}(\theta,\phi), \tag{12}$$

where $\delta_\ell = \pi\mu_\ell$ is the radial phase shift produced due to the presence of the core, with $\mu_\ell$ being the quantum defect, and $f_{\epsilon\ell}(r)$ and $g_{\epsilon\ell}(r)$ represent the radial regular and irregular Coulomb functions for the excited electron, respectively, given by

$$f_{\epsilon l}(r) = \sqrt{\frac{2}{\pi k(r)}} \sin\left(\int^r k(r')dr' + \frac{1}{4}\pi\right), \tag{13}$$

$$g_{\epsilon l}(r) = -\sqrt{\frac{2}{\pi k(r)}} \cos\left(\int^r k(r')dr' + \frac{1}{4}\pi\right), \tag{14}$$

so that $g_{\epsilon l}(r)$ lags $\pi/2$ in phase behind $f_{\epsilon l}(r)$.

To find a transformation relation of the wave functions in spherical and parabolic coordinates, Harmin defined an irregular parabolic wave function $\overline{v}(\eta)$ lagging $\pi/2$ in phase behind $v(\eta)$ in the *Coulomb region*, in a way similar to the definition of irregular Coulomb functions [see Eq. (14)]. However, Harmin shows that the phase accumulation beyond the Coulomb region leads to the following behavior at $\eta \to \infty$:

$$\overline{v}(\eta) \to \sqrt{\frac{2}{\pi k(\eta)}} \sin\left(\int^\eta k(\eta')d\eta' + \frac{1}{4}\pi + \delta_\beta - \gamma_\beta\right), \tag{15}$$

where $\gamma_\beta$ is the asymptotic relative phase shift [relative to the phase of the regular parabolic wave function; see Eq. (7)], which lies in the range $0 < \gamma_\beta < \pi$. The total irregular parabolic eigenfunction is denoted as

$$\chi_{\epsilon n_1 m}(\xi,\eta,\phi) = \frac{u_\beta(\xi)}{\sqrt{\xi}} \frac{\overline{v}_\beta(\eta)}{\sqrt{\eta}} \frac{e^{im\phi}}{\sqrt{2\pi}}. \tag{16}$$

The orthonormalization relation of the parabolic eigenfunctions, and the Wronskian of $v(\eta)$ and $\overline{v}(\eta)$ are expressed as follows in Harmin's work:

$$\begin{aligned} \langle \psi_{\epsilon' n_1' m'} | \psi_{\epsilon n_1 m} \rangle &= \langle \chi_{\epsilon' n_1' m'} | \chi_{\epsilon n_1 m} \rangle \\ &= \delta(\epsilon' - \varepsilon)\delta_{n_1' n_1}\delta_{m' m}, \end{aligned} \tag{17}$$

$$\begin{aligned} \langle \psi_{\epsilon' n_1' m'} | \chi_{\epsilon n_1 m} \rangle &= \langle \chi_{\epsilon' n_1' m'} | \psi_{\epsilon n_1 m} \rangle \\ &= \cos\gamma_\beta \delta(\epsilon' - \varepsilon)\delta_{n_1' n_1}\delta_{m' m}, \end{aligned} \tag{18}$$

$$W_\eta(v_\beta, \overline{v}_\beta) = 2/\pi \sin\gamma_\beta. \tag{19}$$

Here it should be mentioned that the integrals involving $\chi_{\epsilon n_1 m}$ have to be defined cautiously, as the function $\chi_{\epsilon n_1 m}$ diverges at the origin.

In the Coulomb region, Harmin introduced the parabolic Green's function and utilized the equivalence of the parabolic and spherical Green's function to relate the irregular wave functions with the boundary conditions, the orthonormalization relations, and the Wronskian of $v(\eta)$ and $\overline{v}(\eta)$, prescribed in Eqs. (17)–(19). The resulting transformation relation is

$$\mathcal{G}_{\epsilon\ell m}(\mathbf{r}) = \sum_\beta \csc\gamma_\beta \widetilde{U}_{\ell\beta} \chi_\beta(\mathbf{r}), \tag{20}$$

where $\widetilde{U}$ denotes the transpose of the matrix $U$. The regular and irregular wave functions in parabolic and spherical coordinates for nonhydrogenic alkali-metal atoms are connected with the use of Eqs. (8) and (20), respectively.

### B. Harmin's choice of irregular wave functions

This section reviews critically the irregular wave functions defined by Harmin. Obviously, such an irregular solution is not something that is defined uniquely. Any linear combination of $v_\beta(\eta)$ and $\bar{v}_\beta(\eta)$ is also an irregular solution. The choice of the specific irregular solution should be based on the outgoing-wave (incoming-wave) boundary condition, that is, the outgoing (incoming) wave solution should have the following asymptotic form:

$$v_\beta^\pm(\eta) \to \sqrt{\frac{2}{\pi k(\eta)}} \exp\left[\pm i\left(\int^\eta k(\eta')d\eta' + \delta_\beta\right)\right]. \tag{21}$$

As is well known, the theory may also be formulated in terms of the standing-wave Green's function. Then the irregular solution should be chosen as

$$\bar{v}_\beta^{\mathrm{SW}}(\eta) = -\mathrm{Re}\{v_\beta^+(\eta)\} \tag{22}$$

i.e., $\bar{v}_\beta^{\mathrm{SW}}(\eta)$ is lagging $\pi/2$ in phase behind $v_\beta(\eta)$ in the asymptotic region, but not in the Coulomb region. It is apparent that $\bar{v}_\beta^{\mathrm{SW}}(\eta)$ does not correspond to Harmin's $\bar{v}(\eta)$ which is defined in terms of its behavior in the *Coulomb* region, but not in the asymptotic region. It is easy to see that the asymptotic behaviors of $\bar{v}_\beta^{\mathrm{SW}}(\eta)$ and Harmin's $\bar{v}_\beta(\eta)$ are not identical if the states are close to, but not exactly on, Stark resonances, i.e., if the relative phase shift is close to, but not exactly, $\pi/2$.

There is another problem in the frame-transformation theory noticed by Stevens *et al.* [13]: the phase in the left-hand side of Eq. (20) is shifted uniformly with respect to the spherical angle $\theta$, but the corresponding shift in the right-hand side is not uniform in $\theta$. Accordingly, if the phase of the parabolic function $\overline{v}_\beta(\eta)$ is uniformly shifted relative to that of $v(\eta)$, the frame transformation for the irregular function, Eq. (20), results in a $\mathcal{G}_{\epsilon\ell m}$ different from the result of exact numerical calculations. We will illustrate in Sec. V, where some numerical examples will be presented, that the exact irregular wave function is significantly different from the transformed irregular wave function defined by Harmin.

We conclude that the exact irregular solution with a given asymptotic boundary condition can be obtained only by backward integration or by using integrals containing the Green's function (see, e.g., Ref. [23] for details). The coupled-channel theory developed in Ref. [24] is completely equivalent to such a procedure. As was noticed by Stevens *et al.* [13], the deficiency of the frame transformation for the irregular solution "heals" quickly off the $z$ axis, but may be a limiting factor in precision calculations.

## III. FORMULATION OF THE OUTGOING WAVE

### A. Solutions of the homogeneous Schrödinger equation

In this section, we utilize the frame transformation described in the preceding section to formulate parabolic standing-wave solutions and incoming and outgoing solutions of the homogeneous Schrödinger equation. As exhibited in Ref. [24], for alkali-metal atoms with a closed core and a valence electron in highly excited states, the parabolic standing-wave solution expanded in partial waves can be written as

$$\Psi_{\epsilon\beta m} = \sum_{\beta'} \Xi_{\beta'}(\xi)\frac{1}{\sqrt{\eta}}F_{\beta'\beta}(\eta)\Phi_m(\phi), \tag{23}$$

where the indices $\beta'$ and $\beta$ identify the *channel* and *solution*, respectively, $\Xi_{\beta'}(\xi) = u_{\beta'}(\xi)/\sqrt{\xi}$, and $\Phi(\phi) = \exp(im\phi)/\sqrt{2\pi}$ as given in Eq. (1). We will explore now the behavior of $F_{\beta'\beta}$ outside the core region. This function, valid in both the Coulomb-field and Coulomb-Stark regions, is written as a linear combination of regular $v$ and irregular $\overline{v}$ parabolic solutions with an unknown coefficient $\mathcal{R}_{\beta'\beta}$,

$$F_{\beta'\beta} = v_{\beta'}\delta_{\beta'\beta} - \overline{v}_{\beta'}\mathcal{R}_{\beta'\beta}, \tag{24}$$

where $v$ and $\overline{v}$ have the same asymptotic forms as those given in Eqs. (7) and (15), but the semiclassical phase shifts therein should be replaced by the corresponding quantum phase shifts. We will show below how the unknown coefficient is determined in terms of a frame transformation between parabolic and spherical wave functions. Substituting the above expression into Eq. (23), one obtains with the help of Eqs. (1) and (16)

$$\Psi_{\epsilon\beta m}(\mathbf{r}) = \sum_{\beta'}[\psi_{\epsilon\beta m}(\mathbf{r})\delta_{\beta'\beta} - \chi_{\epsilon\beta' m}(\mathbf{r})\mathcal{R}_{\beta'\beta}], \tag{25}$$

where the subscript $n_1$ of $\psi$ and $\chi$ in Eqs. (1) and (16) is replaced by $\beta$. Such a replacement does not cause any confusion. This expression can be considered as the parabolic standing-wave solution. The solution of the Schrödinger equation for alkali-metal atoms in the absence of electric fields is needed to determine the unknown coefficient $\mathcal{R}_{\beta'\beta}$. The spherical standing-wave solution in the Coulomb region, where the frame transformation is performed, is of the form

$$\Theta_{\epsilon\ell m}(\mathbf{r}) = \mathcal{F}_{\epsilon\ell m}(\mathbf{r}) - \tan(\pi\mu_\ell)\mathcal{G}_{\epsilon\ell m}(\mathbf{r}). \tag{26}$$

Note that Eq. (10) used by Harmin is related to Eq. (26) by $\overline{\Theta}_{\epsilon\ell m} = \cos\delta_\ell\Theta_{\epsilon\ell m}$. Multiplying both sides of Eq. (26) by $U_{\beta\ell}$ and summing over $\ell$, one obtains with the aid of Eqs. (8), (12), and (20)

$$\sum_\ell U_{\beta\ell}\Theta_{\epsilon\ell m}(\mathbf{r}) = \sum_{\beta'}\Bigg[\psi_{\epsilon\beta m}(\mathbf{r})\delta_{\beta'\beta} - \csc\gamma_{\beta'} \times \sum_\ell U_{\beta\ell}\tan(\pi\mu_\ell)\widetilde{U}_{\ell\beta'}\chi_{\epsilon\beta' m}(\mathbf{r})\Bigg]. \tag{27}$$

If we define

$$\csc\gamma_{\beta'}\sum_\ell U_{\beta\ell}\tan(\pi\mu_\ell)\widetilde{U}_{\ell\beta'} = \mathcal{R}_{\beta'\beta}, \tag{28}$$

the two equations (25) and (27) are equivalent. Thus we have determined the unknown coefficient $\mathcal{R}_{\beta'\beta}$, and therefore the parabolic standing-wave solutions outside the core region. From the above equations, $\mathcal{R}$ can be regarded as the reaction matrix in parabolic coordinates. Here we would point out that our way of determining the reaction matrix is similar to those of Sakimoto [19] and Robicheaux and Shaw [22].

For simplicity, we introduce a compact matrix notation, in which Eq. (24) reads

$$F = v - \overline{v}\mathcal{R}, \tag{29}$$

with

$$\mathcal{R} = \csc\gamma U\tan(\pi\mu)\widetilde{U} = \csc\gamma\mathcal{K}, \tag{30}$$

where $F$, $v$, and $\overline{v}$ are row matrices, the trigonometric functions represent diagonal matrices, and $U\tan(\pi\mu)\widetilde{U}$ is denoted as $\mathcal{K}$. The asymptotic regular and irregular parabolic solutions are explicitly needed to formulate the incoming- and outgoing-wave solutions. They may be written as

$$v_\beta(\eta) \to \frac{-i}{\sqrt{2\pi k(\eta)}}[e^{i\varphi_\beta(\eta)} - e^{-i\varphi_\beta(\eta)}], \tag{31}$$

$$\overline{v}_\beta(\eta) \to \frac{-i}{\sqrt{2\pi k(\eta)}}[e^{i[\varphi_\beta(\eta)-\gamma_\beta]} - e^{-i[\varphi_\beta(\eta)-\gamma_\beta]}], \tag{32}$$

where $v_\beta(\eta)$ and the phase $\varphi_\beta(\eta)$ may be calculated by integrating the Schrödinger equations for continuous states, as is done in Ref. [25]. It is convenient to utilize the matrix form of the standing-wave solutions to define the incoming- and outgoing-wave solutions $F^\pm$. Multiplying both sides of Eq. (29) by the matrices $\mp i(I - \csc\gamma e^{\pm i\gamma}\mathcal{K})^{-1}$, we obtain with the aid of Eqs. (31) and (32)

$$F^+ = -iF(I - \csc\gamma e^{i\gamma}\mathcal{K})^{-1} = \tfrac{1}{2}(v^- - v^+\mathcal{S}), \tag{33}$$

$$F^- = iF(I - \csc\gamma e^{-i\gamma}\mathcal{K})^{-1} = \tfrac{1}{2}(v^+ - v^-\mathcal{S}^*), \tag{34}$$

where $I$ is the identity matrix, $e^{\pm i\gamma}$ is the diagonal matrix with diagonal elements $e^{\pm i\gamma_\beta}$, $\mathcal{S}^*$ indicates the conjugate of $\mathcal{S}$, given by

$$\mathcal{S} = (I - \csc\gamma e^{-i\gamma}\mathcal{K})(I - \csc\gamma e^{i\gamma}\mathcal{K})^{-1}, \tag{35}$$

and $v^\pm$ are row matrices with elements

$$v^\pm_\beta = \sqrt{\frac{2}{\pi k(\eta)}}\, e^{\pm i\varphi_\beta(\eta)}. \tag{36}$$

It is natural to regard $\mathcal{S}$ as the scattering matrix coupling parabolic channels. This matrix turns out to be unitary. The proof is given in the Appendix. If one replaces the standing-wave solution $F_{\beta'\beta}$ in Eq. (23) by $F^-_{\beta'\beta}$, the three-dimensional orthonormalized wave function is obtained:

$$\Psi^-_{\epsilon\beta m} = \sum_{\beta'} \Xi_{\beta'}(\xi) \frac{1}{\sqrt{\eta}} F^-_{\beta'\beta}(\eta)\Phi_m(\phi). \tag{37}$$

In matrix notation, the equation reads

$$\Psi^- = i\Psi(I - \csc\gamma\, e^{-i\gamma}\mathcal{K})^{-1}, \tag{38}$$

and we further obtain, using the frame transformation near the core given above,

$$\Psi^- = i\Theta\widetilde{U}(I - \csc\gamma\, e^{-i\gamma}\mathcal{K})^{-1}, \tag{39}$$

where $\Psi^-$, $\Psi$, and $\Theta$ are row matrices. The expression gives the connection relation between parabolic and spherical eigenfunctions.

### B. Outgoing wave functions with the atom–radiation-field interaction

The solution of the inhomogeneous Schrödinger equation, namely, the Schrödinger equation with a source describing the interaction between the atom and radiation field, is the outgoing wave function, which has been theoretically proven to be [24]

$$\Psi_{\text{out}}(\mathbf{r}) = -i\pi \sum_{\beta' m} \mathcal{D}^-_{\beta' m}\, \Xi_{\beta'}(\xi) \frac{v^+_{\beta'}(\eta)}{\sqrt{\eta}} \Phi_m(\phi), \tag{40}$$

where $\mathcal{D}^-_{\beta' m}$ is the dipole matrix element for a transition from the initial state to a final state $\Psi^-_{\epsilon\beta' m}$, and is given by

$$\mathcal{D}^-_{\beta m} = \int_0^\infty [\Psi^-_{\epsilon\beta m}(\mathbf{r})]^* D\Psi_{\text{ini}}(\mathbf{r})d\mathbf{r}. \tag{41}$$

It should be mentioned that the constant factor in the expression of $\Psi_{\text{out}}$ is different from that of Ref. [24]. The difference is due to the different coordinate systems. In the present paper, the $\xi$ parabolic coordinate ($\xi = r + z$) is used in order to correspond to Harmin's frame transformation, while the $\xi$ semiparabolic coordinate ($\xi = \sqrt{r+z}$) is used for computation convenience in Ref. [24]. It can be shown that the expression for the outgoing wave function (40) reduces to that for H atoms, as given in Ref. [25], if the quantum defect goes to zero. Substituting Eq. (39) into the above equation, one is able to express the parabolic dipole matrix element in terms of the spherical dipole matrix element $\langle\Phi_{\epsilon\ell m}|D\Psi_{\text{ini}}\rangle$, transformation matrices $U$, relative phase shifts $\gamma$, and quantum defects $\mu$. $\langle\Phi_{\epsilon\ell m}|D\Psi_{\text{ini}}\rangle$ and $\mu$ may be calculated by directly integrating the radial Schrödinger equation or using the $R$-matrix code, as is done in Ref. [26], while calculations of $U$ are illustrated in Sec. V.

Equations (40) and (41) give the outgoing-wave solution

$$\Psi_{\text{out}}(\mathbf{r}) = \int G^+(\mathbf{r},\mathbf{r}')D\Psi(\mathbf{r}')d\mathbf{r}' \tag{42}$$

of the inhomogeneous equation

$$(\epsilon - H)\Psi(\mathbf{r}) = D\Psi_{\text{ini}}(\mathbf{r}) \tag{43}$$

where $H$ is the total Hamiltonian, and $G^+(\mathbf{r},\mathbf{r}')$ is the Green's function corresponding to the outgoing-wave boundary condition. As obvious from the above equations, at $\eta > \eta'$ the Green's function can be written as

$$G^+(\mathbf{r},\mathbf{r}') = -i\pi \sum_{\beta m} [\Psi^-_{\epsilon\beta m}(\mathbf{r}')]^*\, \Xi_\beta(\xi) \frac{v^+_\beta(\eta)}{\sqrt{\eta}} \Phi_m(\phi). \tag{44}$$

It should be emphasized that the principal difference between the frame-transformation theory (FTT) formulated in the present paper and the coupled-channel theory (CCT) [24] lies in calculations of the dipole matrix elements $\mathcal{D}^-_{\beta m}$ [see Eq. (41)] involved in the expression of the outgoing wave function, Eq. (40). In the FTT, $\mathcal{D}^-_{\beta m}$ are evaluated from the frame transformation of wave functions, whereas in the CCT, they are obtained directly by numerical integration of coupled-channel equations with appropriate boundary conditions at the origin and infinity.

### C. Electron current density and differential cross sections

The measurement of differential cross sections in photoionization provides a much more stringent test of theories than the measurement of total photoionization cross sections.

TABLE I. Separation constants $\beta$, transformation coefficients $a_{\beta\ell}$ with $\ell = 2$, normalization amplitudes $N_\xi$ and $N_\eta$, and transformation matrices $U_{\beta\ell}$ at $\epsilon = -154$ cm$^{-1}$, $\mathscr{F} = 880$ V/cm, and $m = 1$. The number in brackets indicates the power of 10.

| $n_1$ | $\beta$ | $a_{\beta\ell}$ | $N_\xi$ | $N_\eta$ | $U_{\beta\ell}$ |
|---|---|---|---|---|---|
| 0 | 3.764 2356[−2] | −2.387 6046[−1] | 3.773 2071[−2] | 1.387 3411[+0] | −1.881 3729[−1] |
| 1 | 7.564 0854[−2] | −2.191 3812[−1] | −5.373 5223[−2] | 1.359 6758[+0] | 2.410 0770[−1] |
| 2 | 1.139 8636[−1] | −1.993 3659[−1] | 6.625 9432[−2] | 1.331 1750[+0] | −2.646 6010[−1] |
| 3 | 1.526 7033[−1] | −1.793 6027[−1] | −7.701 5045[−2] | 1.301 7907[+0] | 2.706 8336[−1] |
| 4 | 1.916 8475[−1] | −1.592 1331[−1] | 8.665 8232[−2] | 1.271 4983[+0] | −2.640 7273[−1] |
| 5 | 2.310 2206[−1] | −1.388 9961[−1] | −9.552 2399[−2] | 1.237 6204[+0] | 2.471 7941[−1] |
| 6 | 2.706 7515[−1] | −1.184 2284[−1] | 1.038 0380[−1] | −9.249 2455[−1] | 1.711 4870[−1] |
| 7 | 3.106 3730[−1] | −9.778 6477[−2] | −1.116 2916[−1] | −1.686 7391[−2] | −2.771 5515[−3] |
| 8 | 3.509 0215[−1] | −7.699 3799[−2] | 1.190 8575[−1] | −3.459 7165[−4] | 4.775 0138[−5] |
| 9 | 3.914 6366[−1] | −5.604 7925[−2] | −1.262 3655[−1] | 9.850 0231[−7] | 1.049 0604[−7] |

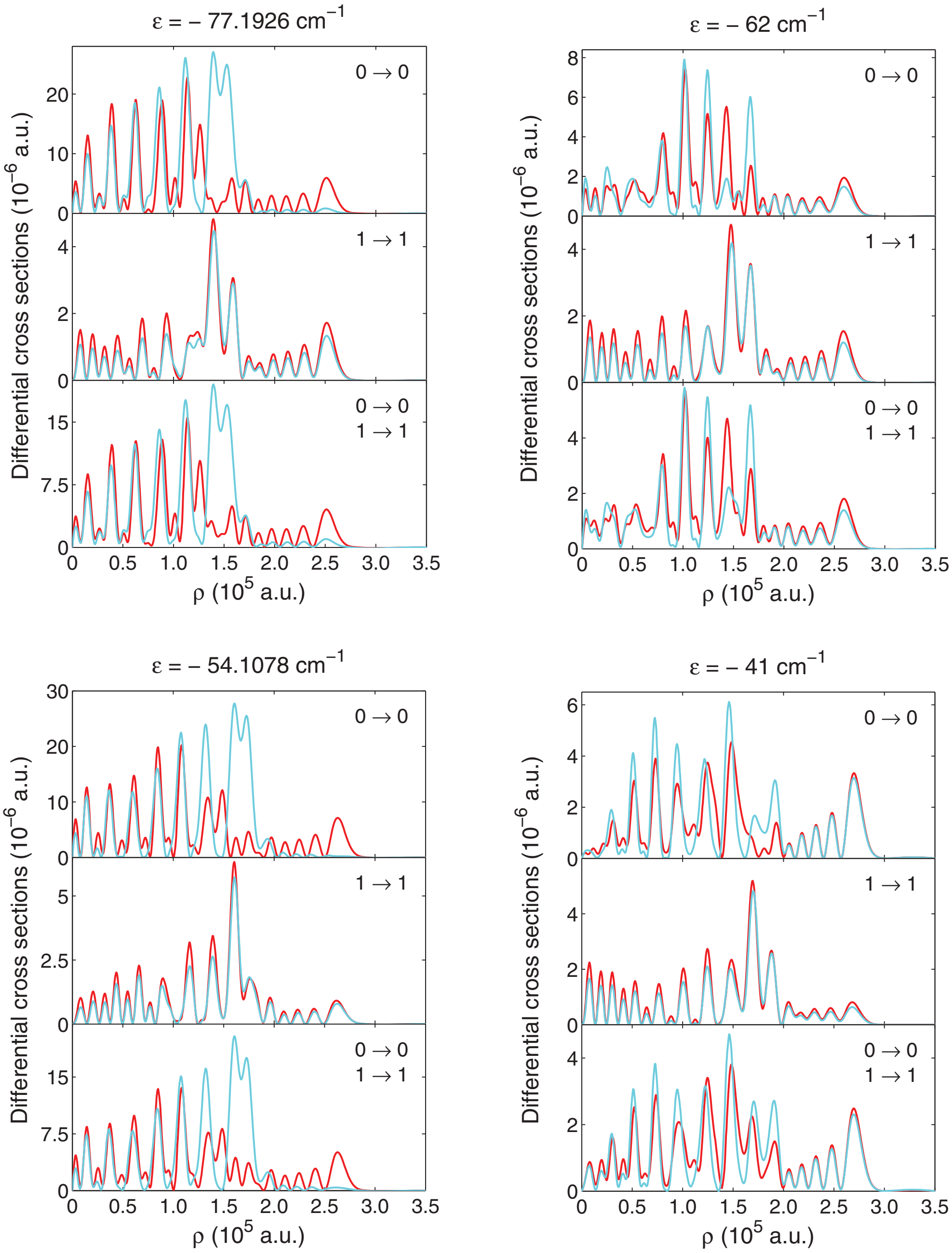

FIG. 1. (Color online) Comparison of differential cross sections from the coupled-channel theory [red (dark gray)] and the frame-transformation theory [cyan (light gray)] of Harmin at four selected energies, in which $-77.1926$ and $-54.1078$ cm$^{-1}$ are right in Stark-resonance locations for the $m = 0$ final states, and $-62$ and $-41$ cm$^{-1}$ are far away from Stark resonances. The ground-state Na atoms placed in an electric field along the $z$ axis with field strength $\mathscr{F} = 3590$ V/cm are photoionized by a two-step transition procedure: they are first excited to the intermediate state $1s^2 2s^2 2p^6 3p\ {}^2P_{3/2}$ by the first $\pi$-polarized laser light beam, and then ionized by the second $\pi$-polarized laser light beam. Due to spin-orbit coupling, the intermediate excited state is a mixture of two pure states $R_{31}Y_{10}$ and $R_{31}Y_{11}$, and therefore the ejected electron currents include contributions from the two states, corresponding to two transitions $m_i = 0 \rightarrow m_f = 0$ and $m_i = 1 \rightarrow m_f = 1$, simply labeled as $0 \rightarrow 0$ and $1 \rightarrow 1$. The curves in the lowest panel for each figure, labeled as both $0 \rightarrow 0$ and $1 \rightarrow 1$, are for $\frac{2}{3}\frac{d\sigma}{d\rho}(m = 0 \rightarrow 0) + \frac{1}{3}\frac{d\sigma}{d\rho}(m = 1 \rightarrow 1)$. The detector is assumed to be located at $z_{\text{det}} = -1000\ \mu$m.

This is precisely the concept of photoionization-microscopy experiments [20,21], where the use of a position-sensitive detector allows the measurement of the differential cross section. Photoionization microscopy allows in fact the direct experimental observation of the squared modulus of the wave function of an electron ejected into the continuum in the presence of a static electric field. In that sense, it provides an extremely demanding test of the various theoretical approaches and offers a unique experimental possibility to challenge the models.

The theoretical formulas for electron current density and differential cross sections have been given in Ref. [24]. They are listed here for convenience. Let us assume that a detector placed under the atomic source in a uniform electric field, and the plane of the detector is perpendicular to the $z$ axis. A dimensionless ratio of the electron current density to the photon current density in cylindrical coordinates ($\rho$, $z$, $\phi$) reads [27,28]

$$\mathscr{R}(\rho,z_{\mathrm{det}},\phi) = \frac{2\pi\omega}{c}\mathrm{Im}\left[\Psi^*(\mathbf{r})\frac{d\Psi(\mathbf{r})}{dz}\right]_{z=z_{\mathrm{det}}}, \tag{45}$$

where $\omega$ is the photon frequency, $c$ is the speed of light, and $z_{\mathrm{det}}$ represents the distance from the origin to the detector. This is in fact the differential cross section, but per unit area, rather than per unit solid angle. This ratio can be integrated over the azimuthal angle $\phi$, and it is convenient to represent the result as a differential cross section per unit length in the $\rho$ variable,

$$\frac{d\sigma(\rho,z_{\mathrm{det}})}{d\rho} = \int_0^{2\pi}\mathscr{R}(\rho,z_{\mathrm{det}},\phi)\rho\,d\phi. \tag{46}$$

## IV. TRANSFORMATION MATRICES AND RELATIVE PHASE SHIFTS

Equation (9) shows that the transformation coefficients $a_{\beta\ell}$ and normalization amplitudes $N_\xi$, $N_\eta$, and $N_\ell$ are needed to obtain transformation matrices. For $a_{\beta\ell}$ and $N_\ell$, the explicit analytical expressions have been given by Harmin [8], and therefore the description of their computational details is omitted here. We illustrate only how $N_\xi$ and $N_\eta$ are calculated using the quantum-mechanical approach. A computational program was written to integrate the Schrödinger equation in mixed semiparabolic and parabolic coordinates with $\zeta = \sqrt{r+z}$ and $\eta = r - z$ [25]. The program is used to compute the semiparabolic eigenfunctions $\mathrm{u}(\zeta)$, while the parabolic eigenfunction $u(\xi)$ can be obtained in terms of the mapping relation $u(\xi)/\sqrt{\xi} = \mathrm{u}(\zeta)/\sqrt{\zeta}$. It should be emphasized that both the semiparabolic coordinate in Ref. [25] and the parabolic coordinate in the present paper are labeled by the same symbol $\xi$ and their eigenfunction also by the same $u(\xi)$. To show the difference and for convenience of discussion,

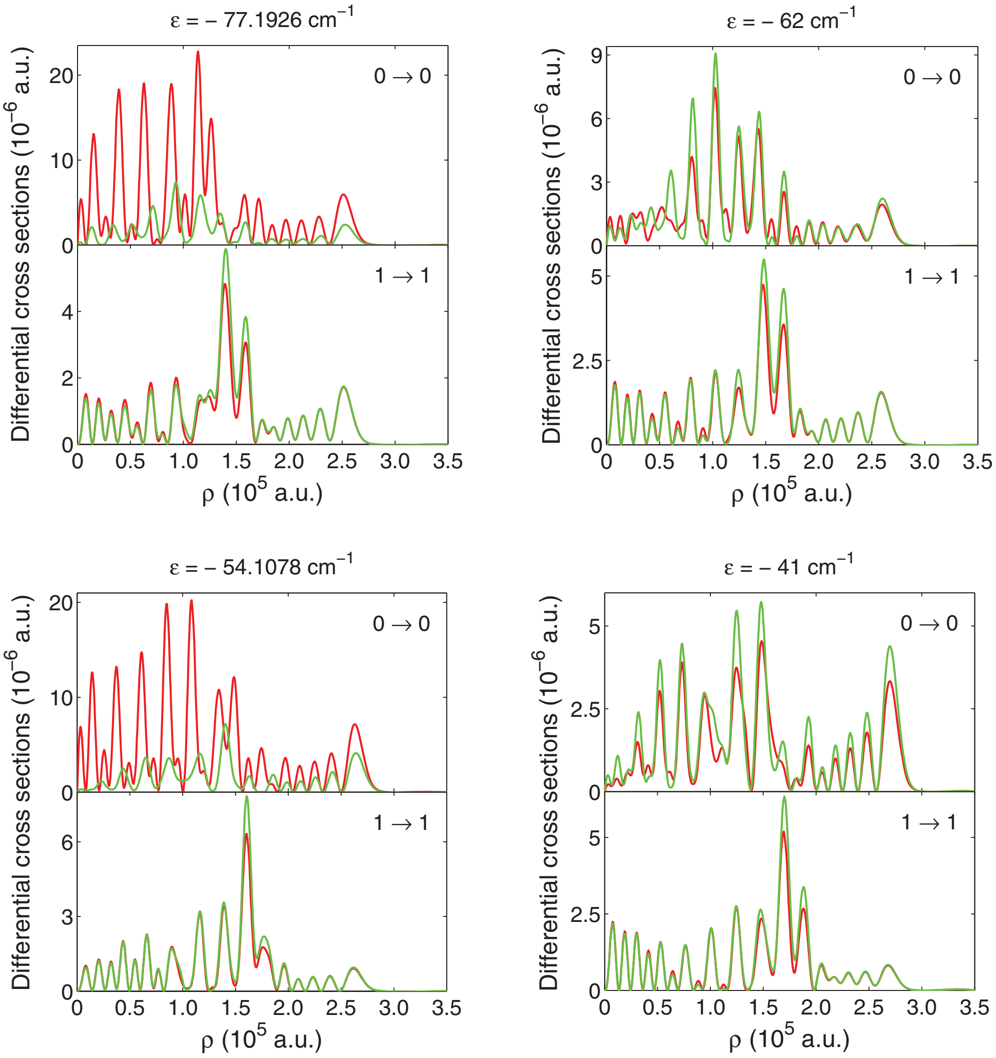

FIG. 2. (Color online) Differential cross sections for Na [red (dark gray)] and artificial H [green (light gray)] atoms calculated in the coupled-channel theory. The laser light beams, the electric field strengths, and the position of the detector are the same as those in Fig. 1. The comparison displays the influence of atomic cores on the differential cross sections or the ejected electron currents.

the semiparabolic coordinate and its eigenfunction used in Ref. [25] are correspondingly changed to $\zeta$ and $\mathrm{u}(\zeta)$ here. Near the origin, the behavior of the normalized $\mathrm{u}(\zeta)$ is [25]

$$\mathrm{u}(\zeta \sim 0) = N_\zeta \zeta^{(1/2+m)}[1 + O(\zeta)], \tag{47}$$

where $N_\zeta$ denotes the normalization amplitude in the semiparabolic coordinate. From the numerical solution of $\mathrm{u}(\zeta)$ and its behavior near the origin indicated in Eq. (47), $N_\zeta$ can be extracted, while the normalization amplitude $N_\xi$ in the parabolic coordinate is readily demonstrated to be $N_\zeta/\sqrt{2}$. The normalization amplitude $N_\eta$ of $v(\eta)$ is extracted from the numerical solution of $v(\eta)$ and its behavior near the origin indicated in Eq. (5).

Table I illustrates the transformation matrices $U_{\beta\ell}$ with $\ell = 2$ and related quantities $\beta$, $a_{\beta\ell}$, $N_\xi$, and $N_\eta$, calculated using the program of Ref. [25] at $\epsilon = -154$ cm$^{-1}$, $\mathscr{F} = 880$ V/cm, and $m = 1$. The corresponding normalization amplitude $N_\ell$ in spherical coordinates is 0.066 432 627 at $\ell = 2$. At this value of $\epsilon$, our calculation shows that the electron waves corresponding to the parabolic quantum states with $n_1 = 0,1,\ldots,6$ propagate above the potential barriers, and the quantum tunneling begins from the quantum state of $n_1 = 7$ and rapidly converges. The values of $N_\eta$ display such a rapid decreasing tendency from $n_1 = 7$ to 10. According to the table, it is sufficient to take a $10 \times 10$ transformation matrix to do a frame-transformation calculation at this value of $\epsilon$.

## V. RESULTS AND DISCUSSION

The outgoing wave functions formulated from the frame-transformation theory of Harmin in the preceding sections are now used to calculate electron current densities and differential cross sections. Let us consider a two-step transition for Na atoms in a uniform electric field. Electrons in the ground state $1s^22s^22p^63s\ ^2S_{1/2}$ are excited first to an intermediate state $1s^22s^22p^63p\ ^2P_{3/2}$ by polarized laser light and then ionized by another polarized laser light. Here these applied laser beams may be of $\sigma^+$ or $\pi$ polarization. A model potential of Na atoms is adopted to describe the interaction between the residual ion (Na$^+$) and the outer valence electron [29]. The reliability of the model potential for the current purpose has been checked by calculating quantum defects for field-free Na atoms. The obtained results are 1.350, 0.859, and 0.022 for $\ell = 0$, 1, and 2, respectively. These values are in good agreement with reported experimental and theoretical data [30]. For the $1s^22s^22p^63p\ ^2P_{3/2}$ state, the Coulomb potential and electron-electron interaction are much stronger than the interaction between the outer valence electron and electric field, so neglecting the electric field is a good approximation for the intermediate state. The radial wave function for this field-free intermediate state is obtained by solving the radial Schrödinger equation in spherical coordinates. The radial integrals of the dipole matrix elements for the $3p \to \epsilon s$ and $3p \to \epsilon d$ transitions in the field-free case are also calculated using this model potential and agree with Harmin's data within 6.5%.

It is apparent that comparison of differential cross sections provides a more stringent test of theories than comparison of total cross sections. In order to test the Stark-effect theory of Harmin, the recently developed coupled-channel theory, which has turned out to be successful in simulating experimental photoelectron currents for Li atoms in an electric field [24], is applied to calculations of differential cross sections for Na atoms, and then the results from the CCT and FTT are compared. A two-step transition procedure of photoionization is selected for ground-state Na atoms placed in a uniform electric field of 3590 V/cm due to irradiation of $\pi\pi$-polarized laser light, namely, $1s^22s^22p^63s\ ^2S_{1/2} \to 1s^22s^22p^63p\ ^2P_{3/2} \to 1s^22s^22p^6 + e$, as described above. For this two-step transition of photoionization, Harmin's theory reproduces the experimental total cross sections (see Ref. [8]). Owing to the spin-orbit coupling, the

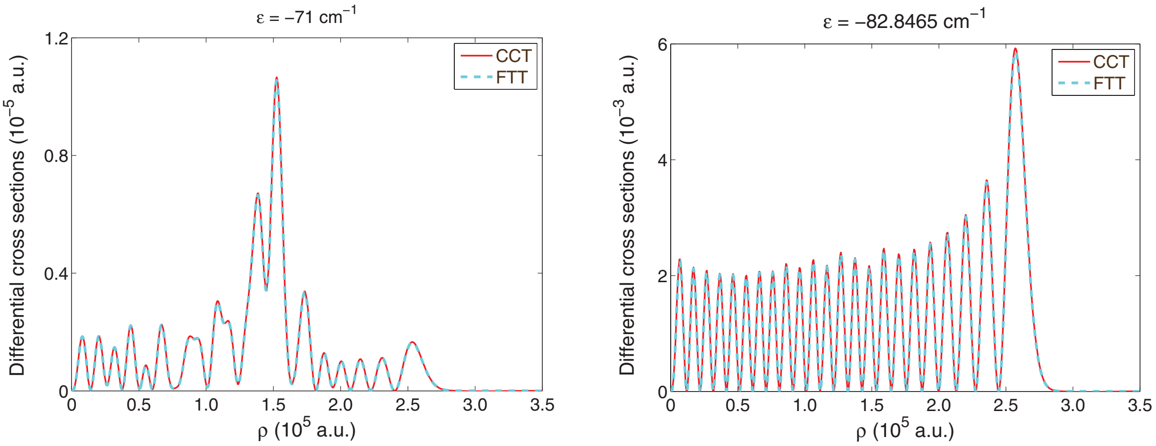

FIG. 3. (Color online) Comparison of differential cross sections from the coupled-channel theory [CCT, red (solid)] and the frame-transformation theory [FTT, cyan (dashed)] of Harmin, applied to H atoms, at two selected energies, in which $-71$ cm$^{-1}$ is far away from Stark resonances, and $-82.8465$ cm$^{-1}$ is right in the Stark resonance $(n_1,n_2,m) = (22,0,1)$. The ground-state H atoms placed in a uniform electric field with field strength $\mathscr{F} = 3590$ V/cm are irradiated by the $\sigma^+\pi$-polarized laser light beams, namely, a two-step transition procedure is assumed: they are first excited to the $2p$ $(m = 1)$ intermediate state, and then ionized by the second $\pi$-polarized laser light beam. In contrast to the case of multielectron Na atoms shown in Fig. 1, the frame-transformation theory of Harmin can exactly reproduce differential cross sections of H atoms.

intermediate state $1s^22s^22p^63p\,^2P_{3/2}$ is a mixture of the two pure states, $R_{31}(r)Y_{10}$ and $R_{31}(r)Y_{11}$; therefore ionization from this intermediate state involves both the $m = 0 \rightarrow 0$ and $m = 1 \rightarrow 1$ transitions. Thus the two-step transition procedure can be regarded as follows: the electron is first excited to the intermediate state $R_{31}(r)[\sqrt{\frac{2}{3}}Y_{10}(\theta,\phi)|\frac{1}{2},\frac{1}{2}\rangle + \sqrt{\frac{1}{3}}Y_{11}(\theta,\phi)\,|\frac{1}{2},-\frac{1}{2}\rangle]$ by the first $\pi$-polarized laser light beam, and then ionized by the second $\pi$-polarized laser light beam, where $|\frac{1}{2},\pm\frac{1}{2}\rangle$ represent two spin states. The differential cross sections from the CCT and FTT are compared in Fig. 1 at four selected energies right in Stark-resonance locations or away from Stark resonances. The differential cross sections from the two theories display obvious discrepancies for the $0 \rightarrow 0$ transitions at the four energies. Such discrepancies should be attributed to frame transformations for irregular wave functions between spherical and parabolic coordinates (See the discussion below for such a comparison).

However, from Fig. 1, one sees only small discrepancies for the $1 \rightarrow 1$ transitions. To explain why the discrepancies are noticeable for the $0 \rightarrow 0$ transitions, but small for the $1 \rightarrow 1$ transitions, let us first analyze atomic core effects in the differential cross sections. We have artificially removed the short-range spherically symmetric core potential defined in Eq. (20) of Ref. [24] to solve the resulting coupled Schrödinger equations, and use the obtained wave functions to compute differential cross sections for an artificial atom which is described by the Na wave function in the initial state and by the H wave function in the final state. This kind of artificial atom is hereafter called the *artificial* H atom. The differential cross sections of the artificial H and real Na atoms are compared in Fig. 2 at these four energies. A much better agreement between the artificial H and real Na atoms is observed for the $1 \rightarrow 1$ transitions than for the $0 \rightarrow 0$ transitions for each energy. This means that the Na atomic core produces a larger effect on the $m = 0$ final state than the $m = 1$ final state. This phenomenon has been interpreted in terms of the orbital penetration effect (see Ref. [24] for detailed discussion). Furthermore, one sees the remarkable discrepancies of the differential cross sections between the artificial H and real Na atoms at energies $\epsilon = -77.1926$ and $-54.1078$ cm$^{-1}$, where the resonances are located for the $m = 0$ final states. Such discrepancies should be attributed to the more pronounced influence of the atomic core under quantum resonance tunneling situations. The presence of the atomic core shifts the resonance positions with respect to the H case. $-77.1926$ and $-54.1078$ cm$^{-1}$ are not resonance locations for H atoms. Now, let us return to Fig. 1. Obviously, the different atomic core effect on the $m = 0$ and $m = 1$ final states is the reason that the discrepancies are noticeable for the $0 \rightarrow 0$ transitions, but small for the $1 \rightarrow 1$ transitions.

In the Stark-effect theory of Harmin, frame transformations between spherical and parabolic coordinates are performed for both regular and irregular wave functions to describe nonhydrogenic atoms [8]. As was discussed in Sec. II and will be shown below, the frame transformations are correct only for the regular wave function but not for the irregular wave function. Thus, we expect that for H atoms in an electric field, the frame transformation used by Harmin should produce exact electron current densities or differential cross sections. To illustrate this conclusion, differential cross sections calculated by the CCT and FTT are drawn in Fig. 3 for H atoms in an electric field of 640 V/cm at the two selected energies. Excellent agreement between the CCT and FTT results is seen for H atoms. It has been shown that Harmin's theory [8] can reproduce experimental photoabsorption spectra (total cross sections) for Na in an electric field of 3590 V/cm. We used the CCT to calculate total cross sections by integrating differential cross sections and found that the experimental photoabsorption spectra for Na are very well reproduced by the present CCT. The experimental and computational photoabsorption spectra are drawn together in Figure 4. The good agreement confirms the reliability of the CCT. We would point out that good agreement of total cross sections for any theoretical approaches

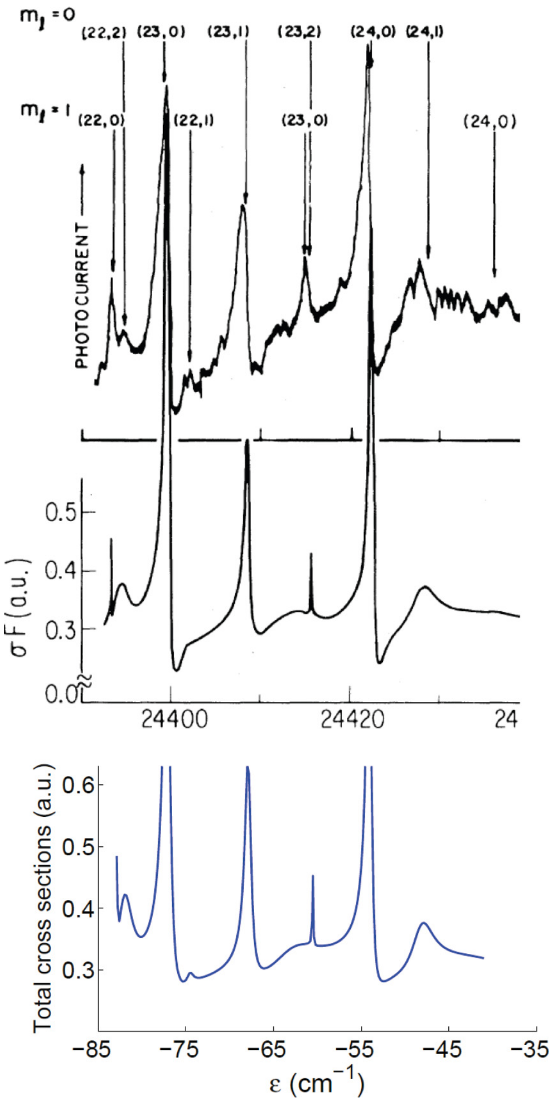

FIG. 4. (Color online) The photoabsorption spectrum for Na atoms in a uniform electric field calculated in the coupled-channel theory. The laser light beams, the electric-field strengths, and the position of the detector are the same as those in Fig. 1. The comparison with experiment confirms the reliability of the coupled-channel theory. The top, intermediate, and bottom panels are experimental [3], Harmin's computational [8], and the present CCT results, respectively. $\sigma^F$ in the intermediate panel denotes the total cross section. This notation is as used by Harmin in Ref. [8].

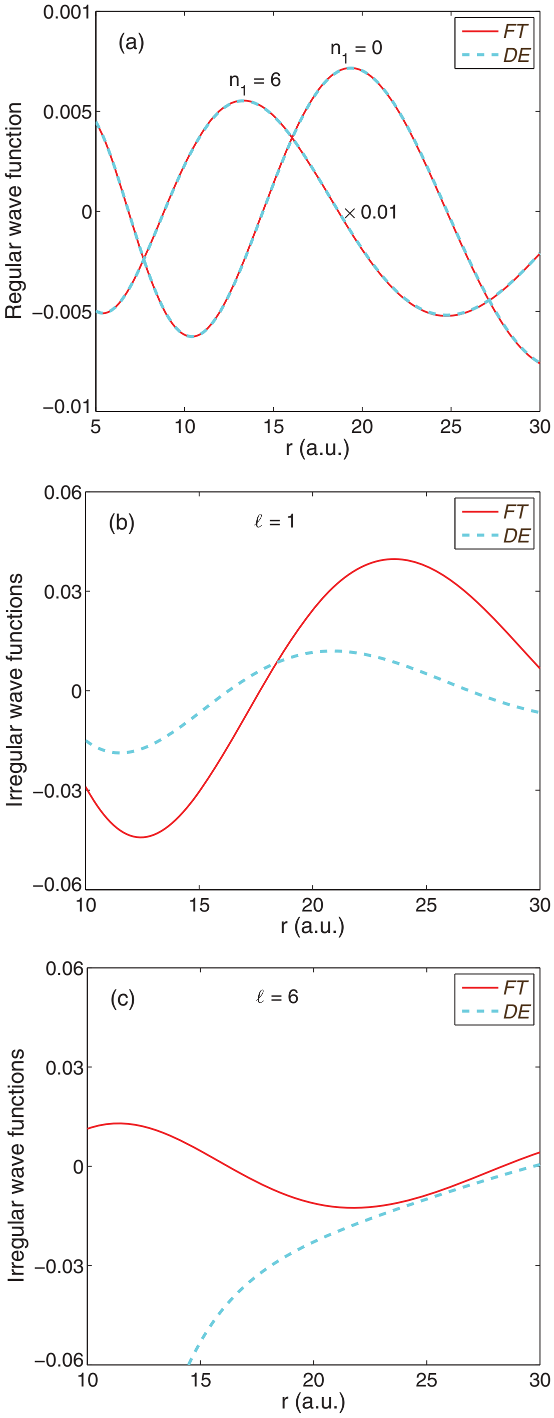

FIG. 5. (Color online) Comparison of frame-transformed (FT) regular and irregular wave functions, given by Eqs. (8) and (20), with wave functions obtained by directly integrating the Schrödinger equation (DE). (a) Regular wave functions; (b) and (c) irregular wave functions. The irregular parabolic wave function has the asymptotic behavior of Eq. (15). We take $\mathscr{F} = 640$ V/cm, $m = 1$, and $\epsilon = 135.8231$ cm$^{-1}$. The two spherical coordinates are fixed to be $\theta = 150^\circ$ and $\phi = 0$.

may conceal some drawbacks of theories themselves, and a more stringent test of theories would be to compare differential cross sections, as is done in Fig. 1.

To check the validity of the frame transformation of the wave functions introduced by Harmin [8], we numerically examined Eqs. (8) and (20) by comparing the transformed and directly calculated regular and irregular wave functions at some energies and electric-field strengths, where the Coulomb wave functions in the spherical coordinate are obtained from Seaton's code [31]. An example at a special energy and electric field is illustrated in Fig. 5. This comparison shows that the frame transformation between parabolic and spherical coordinates produces exact regular wave functions, but the transformed irregular wave function is very poor. This figure helps to explain the existing discrepancies of the differential cross sections between the CCT and FTT results shown in Fig. 1. Obviously, the frame transformation of irregular wave functions introduced by Harmin [8] needs to be further investigated.

## VI. SUMMARY AND CONCLUSION

We formulated outgoing wave functions for photoelectrons produced in photoionization for nonhydrogenic atoms in the presence of a uniform electric field, based on the frame transformation used in Harmin's Stark-effect theory between the spherical and parabolic coordinates. The spatial distributions of electron current densities or differential cross sections for Na are computed and compared to those from a recently developed coupled-channel theory. We analyzed the discrepancies between these two theories and concluded that the frame transformation of irregular wave functions introduced by Harmin is responsible for such discrepancies. Despite its relative inaccuracy in the frame transformation, Harmin's theory has long been proved to be efficient for computing photoionization spectra (i.e., total cross sections) in the presence of an external electric field. It should be pointed out that total cross sections may conceal some drawbacks or limitations of theories themselves, and more detailed physical information may be extracted by comparing detailed differential cross sections, instead of total cross sections. Therefore, photoionization microscopy may become a more useful tool to test the Stark-effect theory. From this point of view, photoionization-microscopy experiments provide a unique experimental possibility to challenge theoretical models. Excellent agreement has already been obtained between the coupled-channel theory and experiment in photoionization of lithium atoms [24], where comparison was limited to the case of excitations far from resonances in order to avoid the peculiarities appearing in quasibound states. In future, comparison between differential cross sections measured on lithium in a photoionization-microscopy experiment with the coupled-channel theory will be extended to the case of Stark resonances, even more challenging for the theory.

## ACKNOWLEDGMENTS

We wish to thank Chris H. Greene and Francis Robicheaux for their critical reviews of our manuscript and helpful comments; we also thank Samuel Cohen for pointing out a reference questioning Harmin's frame transformation (Ref. [13]). This work was supported by the National Science Foundation under Grant No. PHY-0969381 and the National Science Foundation of China under Grant No. 11074260.

## APPENDIX: THE UNITARY PARABOLIC SCATTERING MATRIX

In this Appendix, we prove that the parabolic scattering matrix $\mathcal{S}$ defined in Eq. (35) is unitary, i.e., $\mathcal{S}\mathcal{S}^\dagger = \mathcal{S}^\dagger\mathcal{S} = I$, where $\mathcal{S}^\dagger$ specifies the transpose and conjugate of $\mathcal{S}$. This proof begins from an obvious equality

$$\mathcal{K}\csc\gamma(e^{i\gamma} - e^{-i\gamma}) = \csc\gamma(e^{i\gamma} - e^{-i\gamma})\mathcal{K}, \tag{A1}$$

where $\csc\gamma$ and $e^{\pm\gamma}$ are diagonal matrices with diagonal elements $\csc\gamma_\beta$ and $e^{\pm\gamma_\beta}$, respectively, and $\mathcal{K}$ is the symmetrical matrix given in Eq. (30). Adding $I + \mathcal{K}\csc^2\gamma\mathcal{K}$ on both sides of the equation yields

$$\begin{aligned}(I - \mathcal{K}\csc\gamma e^{i\gamma})&(I - \csc\gamma e^{-i\gamma}\mathcal{K})\\ &= (I - \mathcal{K}\csc\gamma e^{-i\gamma})(I - \csc\gamma e^{i\gamma}\mathcal{K}).\end{aligned} \tag{A2}$$

This equation will be utilized below. From Eq. (35), $\mathcal{S}^\dagger$ is written in the form

$$\mathcal{S}^\dagger = (I - \mathcal{K}\csc\gamma e^{-i\gamma})^{-1}(I - \mathcal{K}\csc\gamma e^{i\gamma}). \tag{A3}$$

Thus

$$\begin{aligned}\mathcal{S}\mathcal{S}^\dagger &= (I - \csc\gamma e^{-i\gamma}\mathcal{K})(I - \csc\gamma e^{i\gamma}\mathcal{K})^{-1}\\ &\quad\times(I - \mathcal{K}\csc\gamma e^{-i\gamma})^{-1}(I - \mathcal{K}\csc\gamma e^{i\gamma})\\ &= (I - \csc\gamma e^{-i\gamma}\mathcal{K})[(I - \mathcal{K}\csc\gamma e^{-i\gamma})\\ &\quad\times(I - \csc\gamma e^{i\gamma}\mathcal{K})]^{-1}(I - \mathcal{K}\csc\gamma e^{i\gamma}).\end{aligned} \tag{A4}$$

Inserting Eq. (A2) into the equation gives

$$\begin{aligned}\mathcal{S}\mathcal{S}^\dagger &= (I - \csc\gamma e^{-i\gamma}\mathcal{K})(I - \csc\gamma e^{-i\gamma}\mathcal{K})^{-1}\\ &\quad\times(I - \mathcal{K}\csc\gamma e^{i\gamma})^{-1}(I - \mathcal{K}\csc\gamma e^{i\gamma}) = I.\end{aligned} \tag{A5}$$

Similarly, it is easy to show that $\mathcal{S}^\dagger\mathcal{S} = I$.

---

[1] T. P. Softley, Int. Rev. Phys. Chem. **23**, 1 (2004).

[2] M. Grütter, O. Zehnder, T. P. Softley, and F. Merkt, J. Phys. B **41**, 115001 (2008).

[3] T. S. Luk, L. DiMauro, T. Bergeman, and H. Metcalf, Phys. Rev. Lett. **47**, 83 (1981).

[4] J. M. Lecomte, S. Liberman, E. Luc-Koenig, J. Pinard, and A. Taleb, Phys. Rev. A **29**, 1929 (1984).

[5] A. König, J. Neukammer, H. Hieronymus, and H. Rinneberg, Phys. Rev. A **43**, 2402 (1991).

[6] D. A. Harmin, Phys. Rev. A **24**, 2491 (1981).

[7] D. A. Harmin, Phys. Rev. Lett. **49**, 128 (1982).

[8] D. A. Harmin, Phys. Rev. A **26**, 2656 (1982).

[9] M. L. Du and J. B. Delos, Phys. Rev. A **38**, 1896 (1988); **38**, 1913 (1988)

[10] J. Gao, J. B. Delos, and M. Baruch, Phys. Rev. A **46**, 1449 (1992); J. Gao and J. B. Delos, *ibid.* **46**, 1455 (1992).

[11] J.-Y. Liu, P. McNicholl, D. A. Harmin, J. Ivri, T. Bergeman, and H. J. Metcalf, Phys. Rev. Lett. **55**, 189 (1985).

[12] P. McNicholl, T. Bergeman, and H. J. Metcalf, Phys. Rev. A **37**, 3302 (1988).

[13] G. D. Stevens, C.-H. Iu, T. Bergeman, H. J. Metcalf, I. Seipp, K. T. Taylor, and D. Delande, Phys. Rev. A **53**, 1349 (1996).

[14] S. D. Hogan and F. Merkt, Phys. Rev. Lett. **100**, 043001 (2008); S. D. Hogan, Ch. Seiler, and F. Merkt, *ibid.* **103**, 123001 (2009).

[15] R. Heidemann, U. Raitzsch, V. Bendkowsky, B. Butscher, R. Löw, L. Santos, and T. Pfau, Phys. Rev. Lett. **99**, 163601 (2007).

[16] S. Willitsch, M. T. Bell, A. D. Gingell, S. R. Procter, and T. P. Softley, Phys. Rev. Lett. **100**, 043203 (2008).

[17] T. Vogt, M. Viteau, A. Chotia, J. Zhao, D. Comparat, and P. Pillet, Phys. Rev. Lett. **99**, 073002 (2007).

[18] H. H. Fielding and T. P. Softley, J. Phys. B **25**, 4125 (1992).

[19] K. Sakimoto, J. Phys. B **19**, 3011 (1986); **22**, 2727 (1989).

[20] C. Nicole, H. L. Offerhaus, M. J. J. Vrakking, F. Lépine, and C. Bordas, Phys. Rev. Lett. **88**, 133001 (2002).

[21] C. Bordas, F. Lépine, C. Nicole, and M. J. J. Vrakking, Phys. Rev. A **68**, 012709 (2003).

[22] F. Robicheaux and J. Shaw, Phys. Rev. A **56**, 278 (1997).

[23] G. A. Gallup, Y. Xu, and I. I. Fabrikant, Phys. Rev. A **57**, 2596 (1998).

[24] L. B. Zhao, I. I. Fabrikant, J. B. Delos, F. Lépine, S. Cohen, and C. Bordas, Phys. Rev. A **85**, 053421 (2012).

[25] L. B. Zhao and J. B. Delos, Phys. Rev. A **81**, 053418 (2010).

[26] L. B. Zhao, A. Ichihara, and T. Shirai, Phys. Rev. A **62**, 022706 (2000); L. B. Zhao and T. Shirai, *ibid.* **63**, 010703 (2000); **64**, 052704 (2001).

[27] I. I. Fabrikant, Sov. Phys. JETP **52**, 1045 (1980).

[28] I. I. Fabrikant, J. Phys. B **23**, 1139 (1990).

[29] J. Hanssen, R. McCarroll, and P. Valiron, J. Phys. B **12**, 899 (1979).

[30] G. L. Snitchler and D. K. Watson, J. Phys. B **19**, 259 (1986).

[31] M. J. Seaton, Comput. Phys. Commun. **146**, 225 (2002); **146**, 250 (2002); **146**, 254 (2002).